Nano Research
2019, 12(7): 1703–1712

ISSN 1998-0124 CN 11-5974/O4
https://doi.org/10.1007/s12274-019-2426-4

Research Article

Two-photon AIE probe conjugated theranostic nanoparticles for tumor bioimaging and pH-sensitive drug delivery

Boxuan Ma[§], Weihua Zhuang[§], Haiyang He, Xin Su, Tao Yu, Jun Hu, Li Yang (✉), Gaocan Li (✉), and Yunbing Wang

National Engineering Research Center for Biomaterials, Sichuan University, Chengdu 610064, China
[§] *Boxuan Ma and Weihua Zhuang contributed equally to this work.*

Received: 21 February 2019 / **Revised:** 23 April 2019 / **Accepted:** 26 April 2019

ABSTRACT

Nanoparticles armed with chemotherapy drug and fluorescence probe have become an effective anticancer strategy for their advantages in cancer diagnosis and treatment. However, fluorophore for diagnostic medicine with deep penetration depth and high resolution are still very rare, while rational designs are also required to improve the tumor retention and target-site drug delivery. Herein, a two-photon fluorophore with aggregation-induced emission and large two-photon absorption cross-section has been designed for two-photon bioimaging, and a novel theranostic nanoplatform is also constructed based on doxorubicin and the two-photon fluorophore conjugated copolymer, P(TPMA-co-AEMA)-PEI(DA)-Blink-PEG ($PAEE_{Blink}$-DA). The micelles maintain a "stealth" property during blood circulation and is activated in the acidic tumor microenvironment, which triggers the charge-conversion and results in enhanced micellar internalization. Meanwhile, PAEMA chains can convert from hydrophobicity to hydrophilicity with accelerated drug release and particle size expansion. The enlarged particle size would potentially extend the retention time of these micelles. Moreover, a great AIE active two-photon bioimaging with tissue penetration depth up to 150 μm is observed and the *in vivo* biodistribution of nanoparticles can be traced. The *in vivo* antitumor results further indicate the obvious reduction of adverse effect and enhanced treatment effect of these micelles, proving that these $PAEE_{Blink}$-DA micelles would be a potential candidate for tumor theranostic applications.

KEYWORDS

polymeric micelle, two-photon, aggregation-induced emission, pH-sensitive, charge conversion, tumor retention

1 Introduction

To date, fluorescent imaging agent has been proven as an important tool in noninvasive cancer diagnosis. In particular, organic fluorescent dyes with controllable emission wavelength are widely developed [1, 2]. Nevertheless, conventional organic fluorescent dyes often suffer from the aggregation-caused quenching (ACQ) effect, which will lead to fluorescence attenuation after accumulation of organic dyes at the target sites [3–5]. Fortunately, a phenomenon of aggregation-induced emission (AIE) has been discovered in 2001 by Tang and his co-workers [6]. These AIE molecules are non-emissive in benign solvents but show strong fluorescent emission in the aggregation state because of the restriction of intramolecular motions, which have been widely employed for bioimaging [3, 7]. Besides the ACQ effect, the conventional single-photon fluorescent dyes are also limited to some extent due to the short excitation wavelength and interference of autofluorescence, which would damage the imaging depth and spatial resolution during the *in vivo* fluorescent imaging [8]. Two-photon fluorescence imaging offers potential for addressing complex physiological and biological challenges rather than cellular events at the single-cell level *in vivo* [2]. It can achieve *in vivo* optical penetration depths up to 1,000 μm and avoid autofluorescence due to the two-photon NIR excitation wavelength range in the biological transparency window, which would be a prior choice for precisely positioning of tumor sites [9]. Moreover, these new-discovered two-photon probes have been confirmed to push the frontiers of fluorescent bioimaging with a larger imaging depth and a clearer spatial resolution [10]. However, reported two-photon probes with aggregation-induced emission are still very rare. Meanwhile, most of traditional two-photon fluorescent dyes widely used for two-photon bioimaging, such as organic dyes, dye-labeled biopolymers and inorganic semiconductor quantum dots, are lacked of chemical modifiability and water-solubility, which limit their further application in *in vivo* bioimaging [7, 11–13] Therefore, the development of more two-photon AIE probes with easy chemical modifiability, deep penetration depth and high resolution is in high demand for excellent fluorescent bioimaging in the diagnostic medicine.

To achieve the long-term circulation in blood stream and a good monodispersity, the fluorescent agents are often encapsulated or conjugated to nanoparticles [7, 14, 15]. Besides loading fluorescent probes for tumor diagnosis, nano-carriers, such as polymeric micelles, can also serve as drug delivery systems to carry anticarcinogen for tumor therapy, constructing the theranostic nanoplatforms against malignant tumors [16–18]. The enhanced permeability and retention (EPR) effect allows nanoparticles with a proper size of < 200 nm to accumulate in tumor tissue during blood circulation, which provides a specific biodistribution of the fluorescent agents and chemotherapy drugs [19]. Nevertheless, the accurate drug delivery into the tumor cells will be another important concern after the drug-loaded micelles accumulate in tumor tissue as the drug-loaded micelles should cross multiple physiological barriers to finally achieve the drug accumulation

Address correspondence to Li Yang, yanglisc@scu.edu.cn; Gaocan Li, gaocanli@scu.edu.cn

in tumor cells [20–22].

In order to efficiently escape from rapid renal clearance by reticuloendothelial system (RES), nano-carriers are usually coated with hydrophilic "stealth" polymers with a neutral or negative charge on the surface, such as polyethylene glycol (PEG) and poly (methacryloyloxyethyl phosphorylcholine) (PMPC) [23–26]. However, when nanoparticles accumulate at tumor site, the negative surface charge or "stealth" polymer coating may hinder the nanoparticle-cell interactions, leading to an unsatisfactory tumor retention and inefficient tumor cellular internalization [20, 27, 28]. From this perspective, nanocarriers are expected to combine with different functions to promote cellular internalization and tumor retention after accumulation in tumor tissue [29–31]. One effective strategy is to endow the nanocarriers a negative-to-positive charge conversional surface and an organized tumor site triggered size expansion (> 200 nm) based on the specific microenvironment of tumor tissue [27, 32–34]. To achieve a satisfactory treatment outcome, smart nanocarriers exploited with stimuli responsiveness have been developed for controlled drug release [35, 36]. Thereinto, tumor exhibits different pH values in its extracellular matrix (6.2–6.8), intracellular lysosome and endosome (~ 5.5), which are quite different with the normal tissue (7.4) [34, 37, 38]. These pH-sensitive structures, such as Schiff base and dimethylmaleic anhydride (DA), have been introduced to the nanocarriers for the enhancement of endocytosis due to their pH-triggered charge conversion ability [29, 39–41]. Meanwhile, some pH-sensitive polymers, for instance, poly (2-azepane ethyl methacrylate) (PAEMA), an ultra pH sensitive polymer, is hydrophobic at pH 7.4 while quickly converts to hydrophilic under pH 6.8, and the drug release can be significantly accelerated in PAEMA-contained nanoparticles due to the hydrophobic-to-hydrophilic transformation. Furthermore, the particle size of the PAEMA-contained nanoparticles would simultaneously change during the hydrophobic-to-hydrophilic transformation to enhance the tumor retention of nanoparticles [42].

Herein, a two-photon fluorophore with AIE property has been designed, which can be simply conjugated to a triblock copolymer P(TPMA-co-AEMA)-PEI(DA)-Blink-PEG ($PAEE_{Blink}$-DA) to develop a theranostic nanoplatform for high-resolution fluorescence bioimaging and efficient tumor elimination. The amino groups of polyethyleneimine (PEI) chain are sheltered by dimethylmaleic anhydride (DA) and polyethylene glycol (PEG) is bridged to the PEI chains by benzoyl imine linkage. Then antitumor drug doxorubicin (DOX) can be loaded into the core of these polymeric micelles. During the blood circulation, the PEG shell is expected to provide satisfactory stability and biosafety while avoiding opsonization and RES clearance. Once the micelles accumulate at tumor sites via EPR effect, the acidic tumor microenvironment would break the benzoyl imine and amide linkage to remove the PEG coating and the DA group linked to PEI chain, respectively. The exposing electropositive amino groups would result in the negative-to-positive charge conversion. Thus, an enhanced cell internalization of micelles and accelerated drug release would be triggered with a stronger antitumor effect. At the same time, the inner PAEMA would also response to the tumor acid environment and turn from hydrophobic to hydrophilic with a micellar expansion, which can lead the micelles trapped inside the tumor tissue and prolong the retention period of micelles (Scheme 1). Accompany with the enhanced tumor retention and tumor site on-demand drug release, a great AIE active two-photon bioimaging in living cell and tissues with the tissue penetration depth up to 150 μm is also observed and the whole process can be monitored. The accelerated and prolonged drug release, and powerful deep fluorescence bioimaging indicate that this nano-sized micelle system can be a promising candidate for distinct fluorescence diagnosis and enhanced chemotherapeutics delivery.

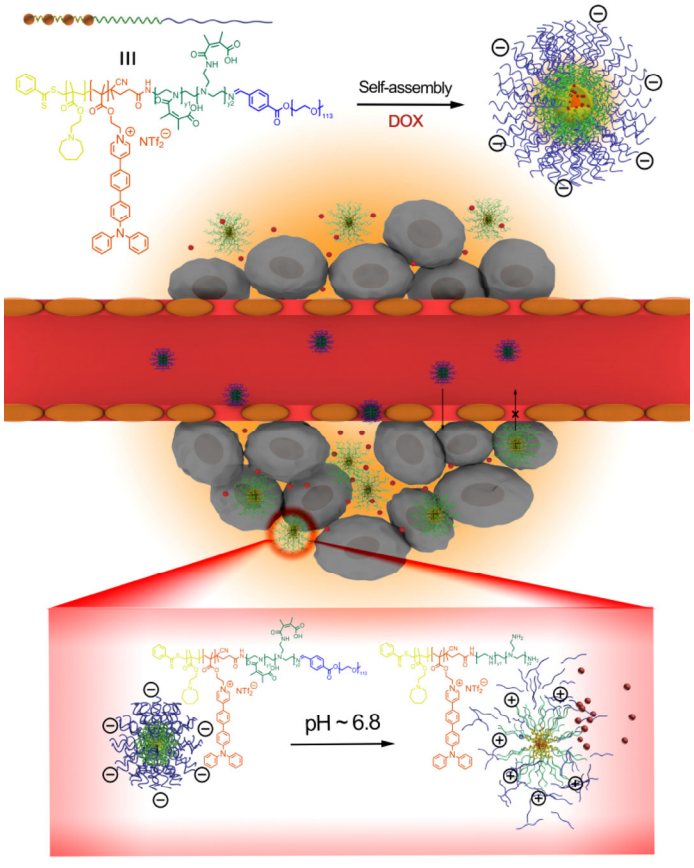

Scheme 1 Illustration of P(TPMA-co-AEMA)-PEI(DA)-Blink-PEG micelles with their pH triggered charge-conversion and drug delivery, along with the two-photon bioimaging.

2 Experimental section

2.1 Synthesis of two-photon fluorophore (TP) and $PAEE_{Blink}$-DA copolymer

Details on the procedure of two-photon fluorophore (TP) and $PAEE_{Blink}$-DA synthesis were described in the Electronic Supplementary Material (ESM).

2.2 Preparation of P(TPMA-co-AEMA)-PEI(DA)-Blink-PEG ($PAEE_{Blink}$-DA) micelles

Doxorubicin (DOX) was firstly obtained by neutralizing DOX·HCl with TEA in DMF. Then 4 mg DOX and 20 mg P(TPMA-co-AEMA)-PEI(DA)-Blink-PEG polymer were dissolved in 4 mL of mixed solvent of DMF, THF and deionized water (1/1/2, v/v/v). After stirred for 1 h, the mixture solution was slowly dropped into 14 mL of deionized water and allowed to stir for another 4 h. Then the solution was dialyzed against deionized water for 48 h in the dark at room temperature, subsequently extruded through a 0.22 μm syringe filter to get the DOX-loaded $PAEE_{Blink}$-DA micelles (1 mg/mL). Analogously, the blank $PAEE_{Blink}$-DA micelles were prepared with the above method.

To investigate the pH-response behavior of the $PAEE_{Blink}$-DA micelles, micellular solution (1 mg/mL) was incubated at pH 7.4 or 6.8, respectively. The zeta potential and the particle size were measured with dynamic light scattering (DLS) at different time intervals. For ^1H NMR spectra, the micelles were incubated at pH 7.4 and 6.8, then dialyzed against deionized water followed by freeze drying.

2.3 *In vitro* drug release behavior of $PAEE_{Blink}$-DA micelles

Lyophilized DOX-loaded micelles were dissolved in DMF and methanol (1/1, v/v) and analyzed by UV spectrophotometry at 480 nm to

calculate drug loading content (DLC) and drug loading efficiency (DLE). Afterwards, the drug release behavior of the micelles was further characterized under different pH. Typically, 2 mL of micellular solution (1 mg/mL) was transferred into a dialysis bag (MWCO = 3,500) along with 20 mL PBS at pH 7.4 or 6.8. The release system was incubated at 37 °C in the dark with sustaining shake. 2 mL sample was withdrawn at selected intervals followed with the addition of 2 mL fresh release medium. The released DOX was also calculated using UV spectrophotometer at 480 nm.

2.4 Aggregation-induced emission (AIE) behavior of $PAEE_{Blink}$-DA micelles

Two-photon fluorophore was introduced for its outstanding fluorescence imaging ability as well as its AIE effect. The AIE behavior of $PAEE_{Blink}$-DA micelles was evaluated by fluorescence spectra in difference ratio of water and THF excited at 410 nm. The concentration of the micelles in various solutions was keeping constant.

2.5 Characterization

^{1}H NMR spectra was performed on a spectrometer operating at 400 MHz (Bruker AMX-400). The particle size and zeta potential of prodrug micelles were recorded by dynamic light scattering (DLS) on a Malvern Zetasizer Nano ZS. The morphology of the micelles was observed by a Hitachi H-600 transmission electron microscope (TEM) with an accelerating voltage of 100 kV and the sample was dyed with 2% phosphotungstic acid before measurement.

2.6 *In vitro* tumor inhibition and apoptosis analysis

In vitro tumor inhibition of DOX-loaded $PAEE_{Blink}$-DA micelles and free DOX·HCl as a contrast were evaluated by MTT assays. Briefly, 4T1 cells were seeded on 96-well plates at a density of 5,000 per well with 200 μL medium and incubated for 24 h. Then the culture mediums were replaced with 200 μL fresh medium at pH 7.4 or 6.8 containing DOX-loaded $PAEE_{Blink}$-DA micelles and free DOX·HCl with various concentrations of DOX ranging from 0.1 to 10 μg/mL. After another 24 or 48 h of incubation, 20 μL MTT solution (5 mg/mL) was added and the cells were incubated for another 4 h. Then the medium was replaced with 200 μL DMSO and the absorbance was measured at 490 nm to investigate the tumor inhibition of the micelles as well as the free drug.

As for apoptosis analysis, 4T1 cells were seeded on 6-well plates at a density of 1.5×10^5 per well and cultured for 24 h before an incubation with $PAEE_{Blink}$-DA micelles and free DOX·HCl (10 μg/mL DOX) for another 24 h at pH 7.4 or 6.8. Then the cells were collected, treated with Annexin V-FITC/PI and analyzed on a BD Accuri C6 flow cytometer.

2.7 *In vitro* cellular uptake and bioimaging

To evaluate the pH-triggered charge conversion of $PAEE_{Blink}$-DA micelles for enhanced cellular uptake, 4T1 cells were seeded on glass dishes (diameter = 35 mm, 1×10^4 cells per dish) with an incubation for 24 h, and then treated with blank $PAEE_{Blink}$-DA micelles (at a two-photon fluorophore dose of 40 μM) at pH 7.4 or 6.8, respectively. After incubated for 2, 4 and 6 h, the cells were washed three times with PBS and observed on a confocal microscope excited at 800 nm. The emission signal in the range of 500–600 nm was collected for bioimaging of the two-photon fluorophore.

Furthermore, flow cytometry was performed to quantitatively measure the pH-responsive cellular uptake of $PAEE_{Blink}$-DA micelles at different pH values. Briefly, 4T1 cells were seeded on 6-well plates (10^6 per well) and incubated for 24 h. Afterwards, blank micelles (at a two-photon fluorophore dose of 40 μM) were added and the cells were incubated for 2 or 4 h at pH 7.4 or 6.8. Then the cells were washed with PBS, trypsinized, centrifuged (1,200 rpm, 5 min), and resuspended in PBS. The fluorescence intensity was measured on a BD Accuri C6 flow cytometer to evaluate the micellular endocytosis.

2.8 Animal experiments

All animal experiments were approved by the Sichuan Provincial Committee for Experimental Animal Management and performed according to the institutional and NIH guidelines for the care and use of research animals. BALB/c mice (female, 20–25 g) were supplied by West China Experimental Animal Center of Sichuan University (China), housed in SPF class animal facility at a controlled temperature of 20–22 °C, relative humidity of 50%–60% and 12 h light-dark cycles with access to commercial rat pellet diet and deionized water ad libitum.

2.9 *Ex vivo* fluorescence imaging

Subcutaneous tumor models were built in the right back of BALB/c mice with 4T1 cells at a density of 10^6. The mice were intravenously injected with solution of blank $PAEE_{Blink}$-DA micelles (at a two-photon fluorophore dose of 1 mM) and were sacrificed after 6, 12, 24 and 48 h after injection. The major organs (heart, lung, liver, spleen and kidney) and the tumor were taken out and imaged by utilizing a Maestro *ex vivo* optical imaging system. Furthermore, after intravenously injection of blank micelles for 12 h, the excised hepatic and nephric tissues were stained with Hoechst 33342 for 30 min at room temperature. Then two-photon fluorescence images of the hepatic and nephric tissues were collected using two-photon CLSM excited at 800 nm.

2.10 *In vivo* tumor inhibition

The mice with subcutaneous tumor models were randomized into three groups (6 mice each group) when the tumor volume reached approximately 100 mm^3 (tumor volume $V = 1/2 \times L \times W^2$, where L and W represented for the length and width of the tumor). Free DOX·HCl, DOX-loaded $PAEE_{Blink}$-DA micelles (5 mg DOX/kg body weight) and saline were separately injected for four times at a time interval of four-day. The tumor inhibition was evaluated by measuring the tumor volume and body weight every two days.

After 21 days, all mice were sacrificed for autopsy and the specimens of mean organs and tumors were excised, fixed with 4% formaldehyde and embedded in paraffin for microscopic examination. Sections were stained with hematoxylin and eosin (H&E) for histopathological analyzation.

2.11 Immunohistochemical analysis of K_i-67, CD31 and TUNEL

Streptavidin peroxidase methods were particularly designed for immunohistochemical (IHC) reactions and other immune evaluation. The tumor sections were deparaffined, rehydrated and incubated overnight at 4 °C with primary monoclonal antibody against CD31 or K_i-67 (1:200) (British Abcam Shanghai Trading Co., LTD). As the secondary antibodies, biotinylated goat anti-rabbit antibodies were used at 1:200 for 30 min at room temperature, and an egg protein reagent marked with horseradish peroxidase was added. The K_i-67 density was calculated as the ratio of K_i-67 positive area to the total area, while the CD31 positive area was expressed in an endothelial cell pack.

As to the TUNEL assay, the rehydrated sections of tumor were incubated with proteinase K at 37 °C for 25 min and rinsed with PBS for three times. The TUNEL assay was carried on *in situ* cell death detection kit-POD (Roche Group, Switzerland) to detect apoptosis. Positive TUNEL staining was observed by optical microscopy, and the apoptotic index was formulated as the ratio of apoptotic cells number to the total tumor cell number.

2.12 Statistical analysis

The contrast between each group were analyzed by a Student's *t* test

to assess statistical significance, where p values of < 0.05 indicated statistical significance. All experiments were performed at least three times and expressed as means ± SD.

3 Results and discussion

3.1 Optical properties of two-photon fluorophore (TP)

The newly designed two-photon fluorophore (**TP**) with AIE feature was prepared via a series of Suzuki reactions following with the subsequent reactions of quaternization and anion exchange as shown in Fig. S1 in the ESM, which was confirmed by NMR spectroscopy and high-resolution mass spectrometry (HRMS) in Figs. S2 and S3 in the ESM (Scheme 2). The fluorophore was consisted of a D-π-A structure with triphenylamine structure as the electron donor and pyridinium group as the electron-accepting moiety. Furthermore, a hydroxyl group was also introduced for the further chemical modification to the drug delivery system. The optical properties of **TP** in different state were investigated and summarized in Fig. 1, Table S1 and Fig. S4 in the ESM. The target fluorophore **TP** showed a very weak emission (λ_{em} = 564 nm) with a fluorescence quantum yield (Φ_f = 0.8%) in THF and a bright emission (λ_{em} = 610 nm, Φ_f = 17.7%) in the solid state (Table S1 in the ESM, Figs. 1(a), 1(d) and 1(e)). Subsequently, the AIE property of **TP** was also investigated by determining the fluorescent intensity of **TP** in the mixture solution of THF and hexane, and a superior AIE performance with the emission enhancement about 19 folds for **TP** was observed (Figs. 1(c) and 1(f)). The two- photon absorption was also observed for **TP**, and a red emission with the emission wavelength at about 605 nm was shown in its THF/ hexane solution (THF/hexane = 1/1, v/v) excited at 840 nm (Fig. 1(b)). Furthermore, the two-photon absorption cross-section of **TP** was also measured relative to a known standard such as Rhodamine B. A large two-photon absorption cross-section up to 265 MG indicated that **TP** could be an ideal probe for *in vivo* two-photon microscopy.

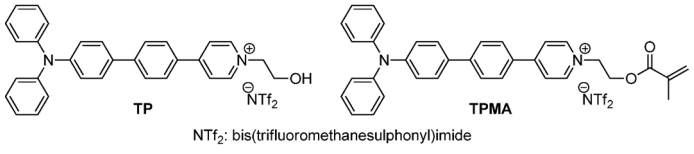

Scheme 2 Chemical structures of TP and TPMA.

3.2 Synthesis of PAEE$_{Blink}$-DA copolymer

PAEE$_{Blink}$-DA copolymer was synthesized via several steps as shown in Fig. 2. The chemical structure of polymerizable two-photon fluorophore monomer TPMA was confirmed by ^{1}H NMR in Fig. S5 in the ESM. Then P(TPMA-co-AEMA) was synthesized via RAFT polymerization. As shown in Fig. 3(a), the degree of polymerization (DP) of AEMA and TPMA were calculated as 8 and 1, and the molecular weight of the copolymer was calculated as 2,750 g/mol.

Afterwards, PEI was conjugated to P(TPMA-co-AEMA) oligomer via amidation reaction with the terminal carboxyl group of copolymers. The characteristic peak of PEI was found at δ 2.52 ppm shown in Fig. 3(b), while peaks a and b belong to P(TPMA-co-PAEMA) polymer. The integral area ratio of peak a, b and c was calculated as 5:16:80, which suggested the successful synthesis of P(TPMA-co-AEMA)-PEI copolymer. The chemical structure of PEG-CHO was confirmed by ^{1}H NMR in Fig. S6 in the ESM, and PEG-CHO was bridged with P(TPMA-co-AEMA)-PEI by a Schiff based reaction. The remaining amino groups of PEI were protected by dimethylmaleic anhydride (DA). As shown in Fig. 3(c), PEG was conjugated to the copolymer with a ratio of about 1:1, while the remaining amino was almost sheltered according to the integral area ratio among peak d, e and c. Therefore, P(TPMA-co-AEMA)-PEI(DA)-Blink-PEG

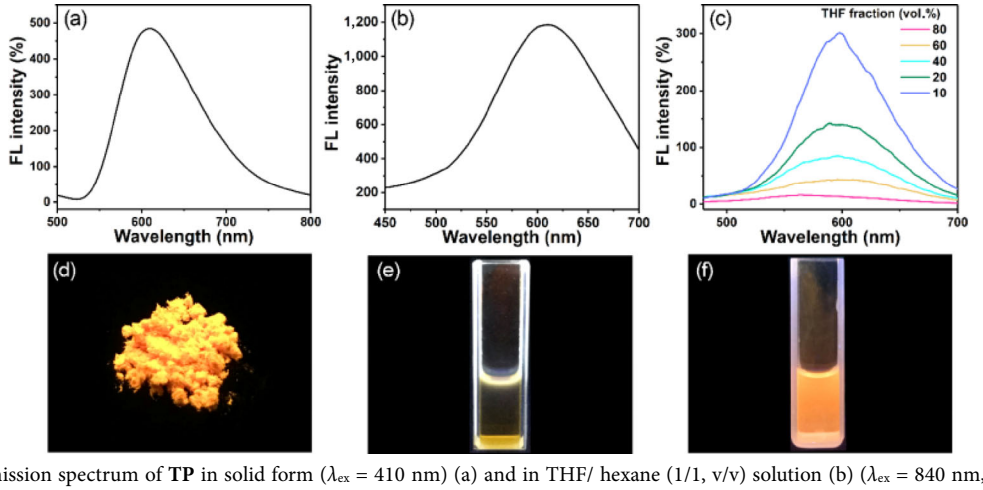

Figure 1 Fluorescent emission spectrum of **TP** in solid form (λ_{ex} = 410 nm) (a) and in THF/ hexane (1/1, v/v) solution (b) (λ_{ex} = 840 nm, excited by a Ti:Sapphire laser). FL spectrum of **TP** in different ratio of THF and hexane (c). Photographs of **TP** in solid form (d), in THF (e) and THF/ hexane (1/1, v/v) solution (f) under UV irradiation at 365 nm.

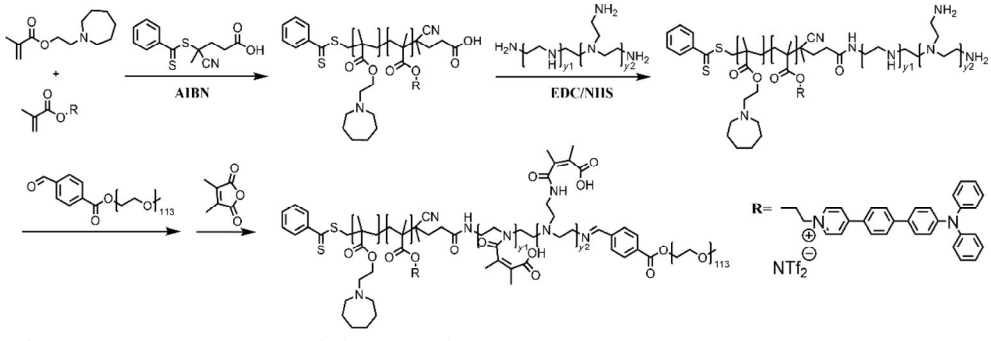

Figure 2 Synthesis route of P(TPMA-co-AEMA)-PEI(DA)-Blink-PEG copolymer.

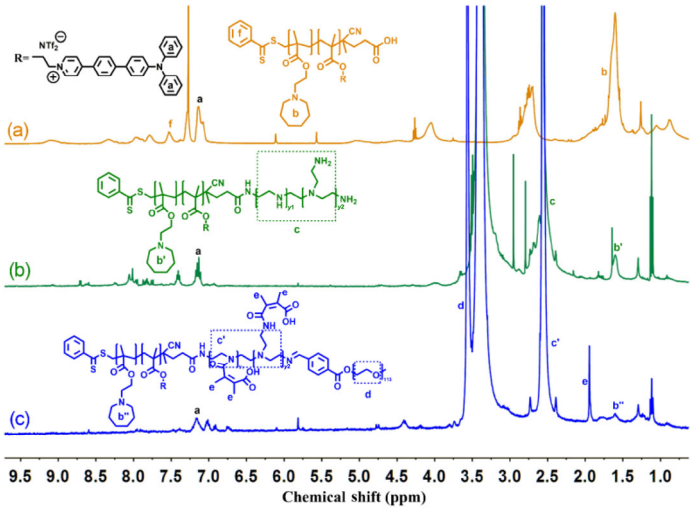

Figure 3 ^{1}H NMR spectra of P(TPMA-co-AEMA) oligomer (a), P(TPMA-co-AEMA)-PEI (b) and P(TPMA-co-AEMA)-PEI(DA)-Blink-PEG (c) copolymer in DMSO-d_6.

copolymer designed in this work could be defined as P(TPMA$_1$-co-AEMA$_8$)-PEI$_{1.8k}$(DA)-Blink-PEG$_{5k}$(M_W ≈ 9,550).

3.3 Preparation of PAEE$_{Blink}$-DA micelles

DOX-loaded PAEE$_{Blink}$-DA micelles were expected to be core-shell structure, which was confirmed by ^{1}H NMR in D_2O (Fig. S7(a) in the ESM). Characteristic peaks of PEG, PEI and DA was clearly observed while peaks of P(TPMA-co-AEMA) were disappeared, indicating a well-defined core-shell structure of these micelles. Furthermore, DOX-loaded PAEE$_{Blink}$-DA micelles showed a tighter micellar structure with a particle size of 75.6 nm and a size distribution (PDI) of 0.112, while the size of blank micelles was about 83.3 nm with a PDI of 0.155 (Fig. 4(a)). The morphology of DOX loaded PAEE$_{Blink}$-DA micelles was further observed by TEM (Fig. 4(b)), which demonstrated a relative uniform spherical morphology of these micelles. The smaller particle size in TEM image than that of DLS was because of the shrinkage of the micellar shell during the sample preparation. On the other hand, the CMC for PAEE$_{Blink}$-DA micelles was determined to be 1.95 μg/mL (Fig. S8 in the ESM), providing these micelles a good stability when diluted by the blood stream after injection.

3.4 pH-responsive behaviors

After accumulation in tumor tissue via EPR effect, the PAEE$_{Blink}$-DA micelles could rapidly respond to the acidic tumor microenvironment, leading to size variation, charge conversion and accelerated drug release. DLS was firstly used to characterize the size variation under acidic condition over time. When at normal physiological pH (7.4), the PAEE$_{Blink}$-DA micelles exhibited a lasting stability for even a month (Fig. S9 in the ESM). However, as shown in Figs. 4(c) and 4(d), the size of PAEE$_{Blink}$-DA micelles increased from 75.6 to 223.2 nm in 2 h at pH 6.8, which might be because PAEMA turned to hydrophilic along with the breaking of DA and PEG (Fig. 4(c)). This result was further proven by ^{1}H NMR in Fig. S7(b) in the ESM, from which the characteristic peaks of PAEMA (δ 1.6 ppm) were found, while the peaks of PEG (δ 3.5 ppm) and DA (δ 2.0 ppm) were disappeared after dialyzing against HCl solution for 48 h (pH 6.0, MWCO = 6,000). The influence of acidic condition to PAEE$_{Blink}$-DA micelles was further investigated by TEM (Fig. 4(e)). A swollen but homogeneous morphology was observed after incubating micelles at pH 6.8 for 4 h, which was in accordance with the result in Figs. 4(c) and 4(d). The DLS and TEM results strongly demonstrated a pH-triggered expansion of the micelles at pH 6.8, which would trap the micelles inside tumor tissue and accelerate DOX delivery, leading to an enhanced therapeutic effect.

Under acidic condition, it was anticipated that the zeta potential of PAEE$_{Blink}$-DA micelles would significantly rise due to the exposed amino groups of PEI and the protonation of PAEMA. As shown in Fig. 4(f), a constant negative surface charge of PAEE$_{Blink}$-DA micelles was detected at pH 7.4 in 6 h, which provided micelles "stealth" property during blood circulation. However, the zeta potential at pH 6.8 increased rapidly, which dramatically reached to 0 mV within 30 min. Then, the zeta potential of the micelles went up to +4.8, +15.2, +16.9 and +17.4 mV at 1, 2, 4 and 6 h, respectively. The sudden charge conversion would result in an enhanced endocytosis of drug-loaded micelles for efficient tumor inhibition.

DOX was loaded into the PAEE$_{Blink}$-DA micelles with DLC of 9.1% and DLE of 49.5%. The pH-triggered transformation of micellar structure would lead to accelerated drug release. The *in vitro* drug release was carried out at pH 6.8 and 7.4 and the accumulative DOX release was shown in Fig. 4(g). When at pH 6.8, more than 50% of the cargo was released within 4 h and about 90% of the DOX was released after 48 h, whereas the drug release under pH 7.4 was much slower with only 26.5% of the cargo release after 48 h. The

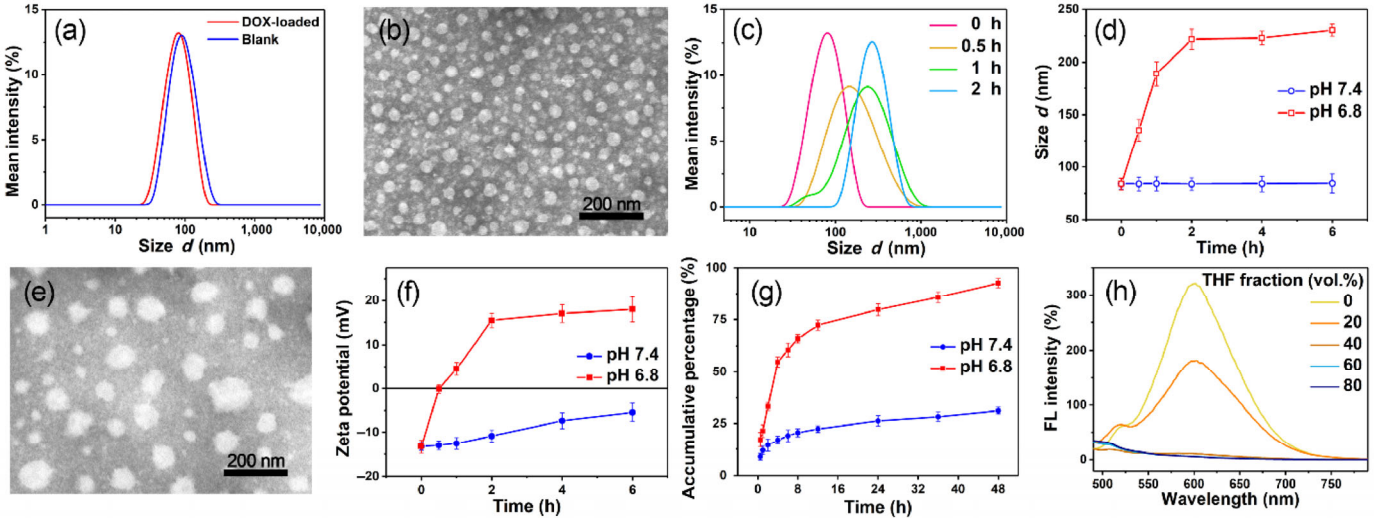

Figure 4 (a) Particle size of blank and DOX-loaded PAEE$_{Blink}$-DA micelles. (b) TEM image of PAEE$_{Blink}$-DA micelles at pH 7.4. (c) Variation trend of particle size at pH 6.8 over time measured by DLS. (d) Size variation of PAEE$_{Blink}$-DA micelles at different pH over time measured by DLS. (e) TEM image of PAEE$_{Blink}$-DA micelles at pH 6.8 for 4 h. (f) Zeta potential variation of PAEE$_{Blink}$-DA micelles at different pH over time measured by DLS. (g) Accumulative DOX release from PAEE$_{Blink}$-DA micelles at pH 7.4 and 6.8. (h) FL spectrum of PAEE$_{Blink}$-DA micelles in different ratio of water and THF.

burst DOX release under acidic environment made these micelles suitable for accurate drug delivery and enhanced treatment effect.

3.5 AIE behavior and two-photon cellular imaging

Two-photon fluorophore labeled $PAEE_{Blink}$-DA micelles were designed to possess AIE feature so as to be applied to bioimaging. As expected, $PAEE_{Blink}$-DA micelles showed great AIE phenomenon. As shown in Fig. 4(h), with the increase of THF fraction from 0% to 20%, the fluorescence intensity reduced sharply. After the THF fraction reached 40% or more, there was nearly no fluorescent emission that could be observed due to the great solubility of the two-photon fluorophore in THF. Furthermore, the AIE feature was also investigated under pH 6.8, and the variation tendency was shown in Fig. S10 in the ESM, where the micelles exhibited great AIE property at both pH 6.8 and 7.4. The strong fluorescence intensity owing to the aggregation of PTPMA exhibited a distinct AIE feature of $PAEE_{Blink}$-DA micelles, which could be a potential fluorescence probe for *in vitro* two-photon cellular imaging.

The two-photon bioimaging ability was further investigated by two-photon CLSM observing 4T1 cells treated with blank $PAEE_{Blink}$-DA micelles for different time excited at 800 nm (Fig. 5). A clear image was obtained after 2 h according to the bright two-photon fluorescence signals of PTPMA. With the extension of time, the internalized micelles increased along with a stronger fluorescence intensity. What's more, compared with the incubation at pH 7.4, the cells exhibited a brighter fluorescence when incubated at pH 6.8 in same time, which suggested that more micelles were endocytosed under acidic condition on account of the pH-triggered charge conversion. Furthermore, this improved endocytosis behavior was also characterized by flow cytometry. After incubation against blank micelles for 2 and 4 h at different pH, more micelles were internalized over time and the acidic environment could accelerate the endocytosis via triggering the charge conversion (Fig. 8(a)), which was in accordance with the CLSM result. The enhanced endocytosis would result in a higher delivery efficiency and a preferable tumor inhibition.

3.6 *Ex vivo* fluorescence imaging

To trace the *in vivo* distribution of $PAEE_{Blink}$-DA micelles after injection, mice were sacrificed after being injected with blank micelles at different time interval. As shown in Fig. 6(a), while no fluorescence was observed in control group, micelles-treated group showed clear fluorescence in livers, kidneys and tumors. The incremental fluorescence intensity at tumor within 48 h indicated that more micelles were accumulated and delayed at tumor site owing to the EPR effect and pH-triggered size expansion of $PAEE_{Blink}$-DA micelles, which was even better than our earlier works [43, 44]. What's more, degressive fluorescence observed in kidneys and livers demonstrated the systemic metabolism of the micelles. The

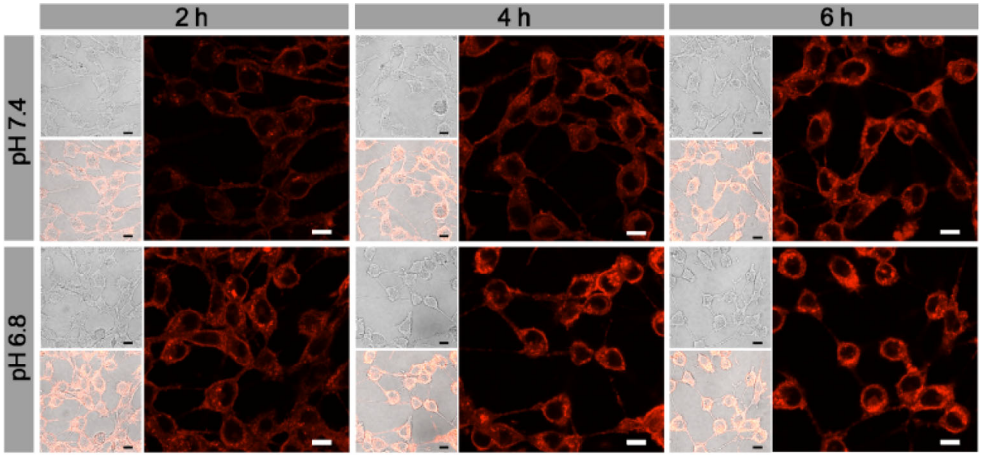

Figure 5 Two-photon CLSM imaging of 4T1 cells cultured with blank $PAEE_{Blink}$-DA micelles for different time excited at 800 nm. The scale bars were 10 μm.

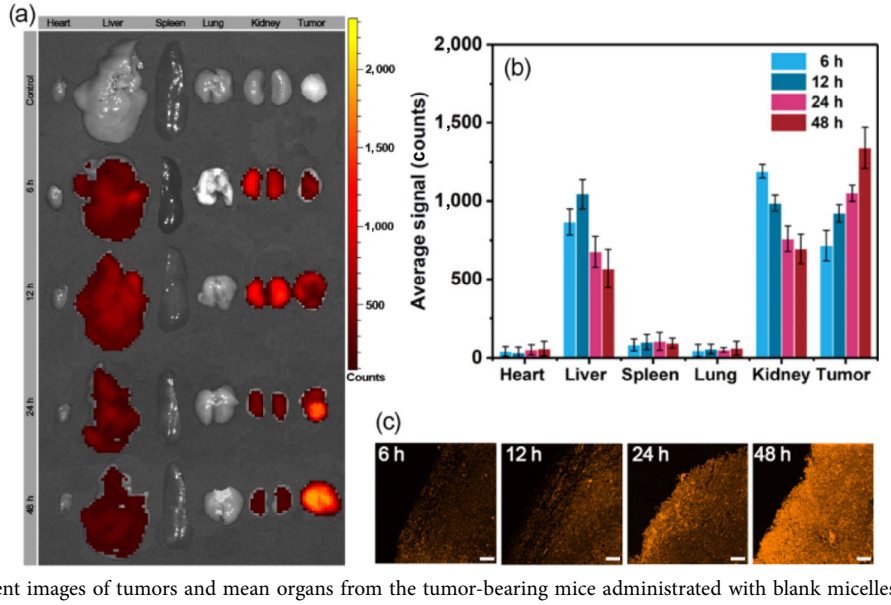

Figure 6 (a) *Ex vivo* fluorescent images of tumors and mean organs from the tumor-bearing mice administrated with blank micelles. (b) Fluorescence intensity of blank $PAEE_{Blink}$-DA micelles in major organs and tumor at different time. (c) Two-photon CLSM images of tumor tissue sections at different time treated with blank $PAEE_{Blink}$-DA micelles. The scale bars were 100 μm.

fluorescence variation was further shown in Fig. 6(b), which was well agreed with the result in Fig. 6(a). Furthermore, the great accumulation and retention of the $PAEE_{Blink}$-DA micelles were also confirmed by observing the section of the tumor tissue with two-photon CLSM excited at 800 nm (Fig. 6(c)), where the fluorescence was found getting stronger as time extended. Therefore, $PAEE_{Blink}$-DA micelles would be a potential candidate for accurate visible cancer treatment.

Furthermore, the outstanding imaging depth of the two-photon microscopy in tissue bioimaging of $PAEE_{Blink}$-DA micelles was evaluated by two-photon CLSM. The hepatic and nephric tissues were chosen for the fluorescence imaging after injection of blank micelles for 12 h. As shown in Fig. 7, a bright fluorescent signal was observed in both hepatic and nephric tissues under 800 nm two-photon excitation. With the depth of scanning increasing, the fluorescence of Hoechst 33342 and micelles under one-photon excitation at 405 nm declined rapidly. However, deeper tissue imaging of the micelles with a depth of up to 150 μm was still visualized under excitation of two-photon laser, which indicated a great potential of these micelles for tissue bioimaging upon two-photon excitation.

3.7 *In vitro* cytotoxicity and tumor inhibition

As an ideal nano-carrier for drug delivery and fluorescent bioimaging, the blank micelles should possess a good biocompatibility, which was evaluated by MTT assays shown in Fig. S11 in the ESM. The relative cell viability of both 4T1 and L929 cells were around 100% even at a dose of 0.25 mg/mL, which demonstrated the excellent biocompatibility of $PAEE_{Blink}$-DA micelles. On the other hand, after DOX loaded, the $PAEE_{Blink}$-DA micelles should exhibit satisfactory antitumor effect. As shown in Fig. 8(b), with the increasing concentration of DOX from 0.1 to 10 μg/mL, the cell viability of 4T1 cells decreased from 68% to 31% in 48 h at pH 7.4, which showed a slight deficiency from the performance of free DOX. However, when at pH 6.8, the DOX-loaded micelles exhibited a similar cell killing behavior compared with free DOX, and the cell viability was reduced

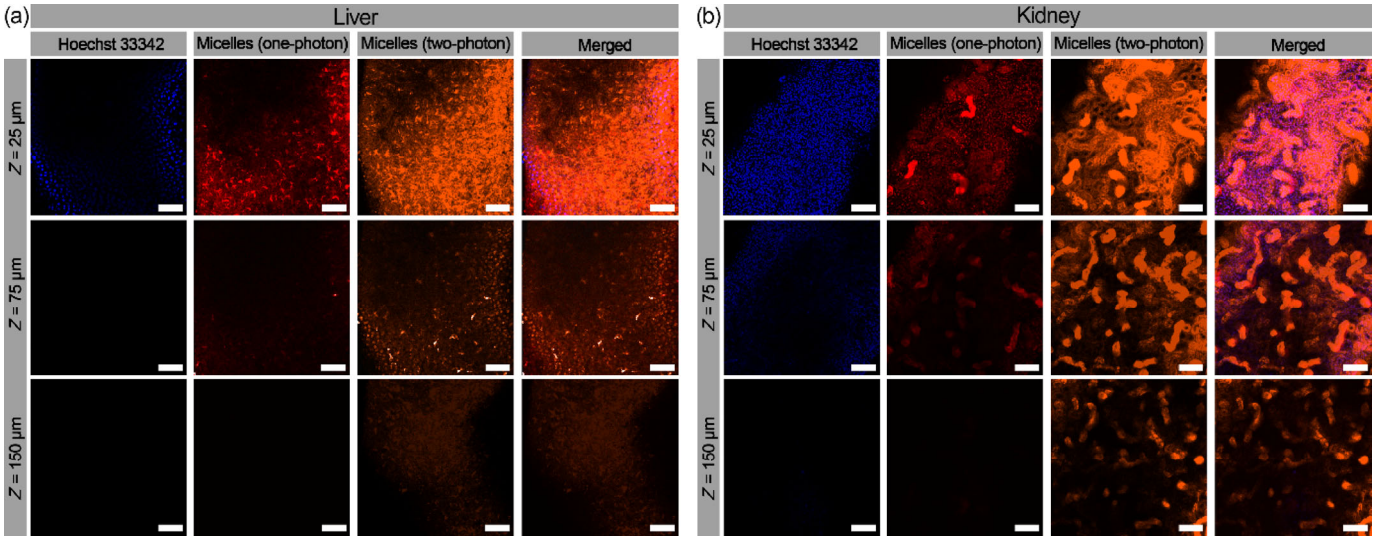

Figure 7 Two-photon CLSM images of the liver (a) and the kidney tissues (b) after injection of blank micelles for 12 h. The scale bars were 100 μm.

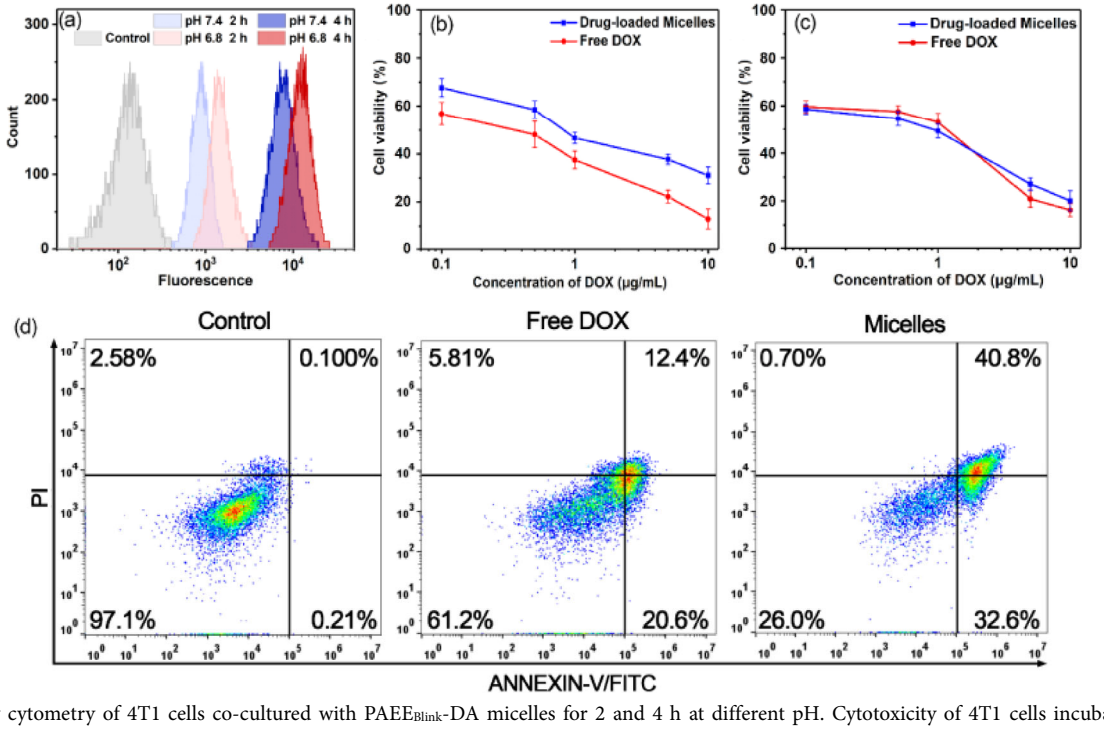

Figure 8 (a) Flow cytometry of 4T1 cells co-cultured with $PAEE_{Blink}$-DA micelles for 2 and 4 h at different pH. Cytotoxicity of 4T1 cells incubated with various concentration of DOX-loaded $PAEE_{Blink}$-DA micelles and free DOX for 48 h at pH 7.4 (b) and 6.8 (c). (d) Cell apoptosis measured by cell cytometry after labeling 4T1 cells with annexin V-FITC/PI at pH 6.8.

to 20% after 48 h with a DOX concentration of 10 μg/mL (Fig. 8(c)).

Furthermore, tumor inhibition was also correlated with the induction of cell apoptosis. As shown in Fig. S12 in the ESM, the drug-loaded PAEE$_{Blink}$-DA micelles and free DOX demonstrated a similar apoptosis on 4T1 cells at pH 7.4, while the PAEE$_{Blink}$-DA micelles exhibited a stronger apoptosis compared with free DOX at pH 6.8 in Fig. 8(d). The DOX-loaded PAEE$_{Blink}$-DA micelles revealed a better tumor inhibition in cell apoptosis and cytotoxicity at pH 6.8 owing to its pH-triggered charge conversion and drug release, which led to the efficient internalization and outstanding anticancer performance.

3.8 *In vivo* antitumor efficacy

To further explore the potential of cancer therapy of these PAEE$_{Blink}$-DA micelles *in vivo*, 4T1 breast cancer tumor-bearing BALB/c mice were treated with free DOX and DOX-loaded PAEE$_{Blink}$-DA micelles at a dose of 5 mg DOX/kg body weight along with saline as the control group after the inoculated tumor volume reached about 100 mm^3. As shown in Fig. 9(a), the control group exhibited no tumor inhibition with a rapid volume growth. In contrast to both saline and free DOX, the PAEE$_{Blink}$-DA micelles showed a stronger tumor growth suppression. Furthermore, body weight loss was another obvious indicator to evaluate DOX-induced toxicity (Fig. 9(b)). When the treatment cycles of 21 days were finished, serious body weight loss emerged in the mice injected with free DOX, where about 14% of body weight was lost. On the other side, no significant variation was observed between micelles treated group and control group, indicating the great biosecurity of these PAEE$_{Blink}$-DA micelles.

3.9 Histological studies and immunohistochemical analysis

In situ histological studies was supportive of the splendid biocompatibility along with the excellent therapeutic efficacy of the PAEE$_{Blink}$-DA micelles. As shown in Fig. S13 in the ESM, focal infiltration of neutrophils and inflammatory cells could be discovered in H&E section of heart, liver, spleen, lung and tumor tissue treated with free DOX, indicating the severe inflammatory reaction and organ toxicity. However, few inflammation and toxicity were noticed in micelles-treated group owing to the favorable biosafety of PAEE$_{Blink}$-DA copolymer. What's more, the highest level of tumor cell apoptosis was observed in micelles-treated group, demonstrating an outstanding tumor inhibition of these PAEE$_{Blink}$-DA micelles.

Furthermore, results of immunohistochemical analysis (CD31, K_i-67 and TUNEL) could also prove the antitumor efficiency of the PAEE$_{Blink}$-DA micelles (Fig. S14 in the ESM). For the micelles-treated group, the fewest angiogenesis, least differentiated cells and most apoptotic cells were found respectively in CD31 (Fig. 9(c)), K_i-67 (Fig. 9(d)) and TUNEL (Fig. 9(e)) assays. The DOX-loaded PAEE$_{Blink}$-DA micelles could effectively inhibit angiogenesis, tumor cell proliferation and induce cell apoptosis, which led to an admirable antitumor effect owing to the rapid accumulation and prolonged retention at tumor tissue of these micelles.

4 Conclusion

In summary, a new two-photon fluorophore with great AIE effect has been designed and synthesized, which emits a bright AIE fluorescence with a large two-photon absorption cross-section. A novel theranostic system has also been developed by introducing the two-photon fluorophore to DOX-loaded PAEE$_{Blink}$-DA micelles for simultaneously two-photon fluorescence imaging and environment promoted antitumor efficacy. The micelles maintain satisfactory stability during blood circulation and can accumulate at tumor sites via EPR effect. Once the micelles expose to the acidic tumor microenvironment, the negative-to-positive charge conversion and the hydrophobic-to-hydrophilic conversion of PAEMA will occur, efficiently accelerating the endocytosis and triggering the rapid drug release. Moreover, the micelles can continually accumulate in tumor sites and the expansion of particle size would help to trap the drug-loaded micelles in the tumor tissue, enhancing the antitumor effect. It is important that DOX-loaded PAEE$_{Blink}$-DA micelles exhibit a great antitumor ability *in vivo* with the minimum side effects. What's more, great biocompatibility and deep two-photon tissue bioimaging (up to 150 μm) has also been proven for blank PAEE$_{Blink}$-DA micelles. The great biocompatibility, deep two-photon tissue bioimaging, enhanced antitumor effect and minimum side effects make this theranostic DOX-loaded PAEE$_{Blink}$-DA micelle system a great promise for fluorescent imaging-guided cancer therapy and diagnosis.

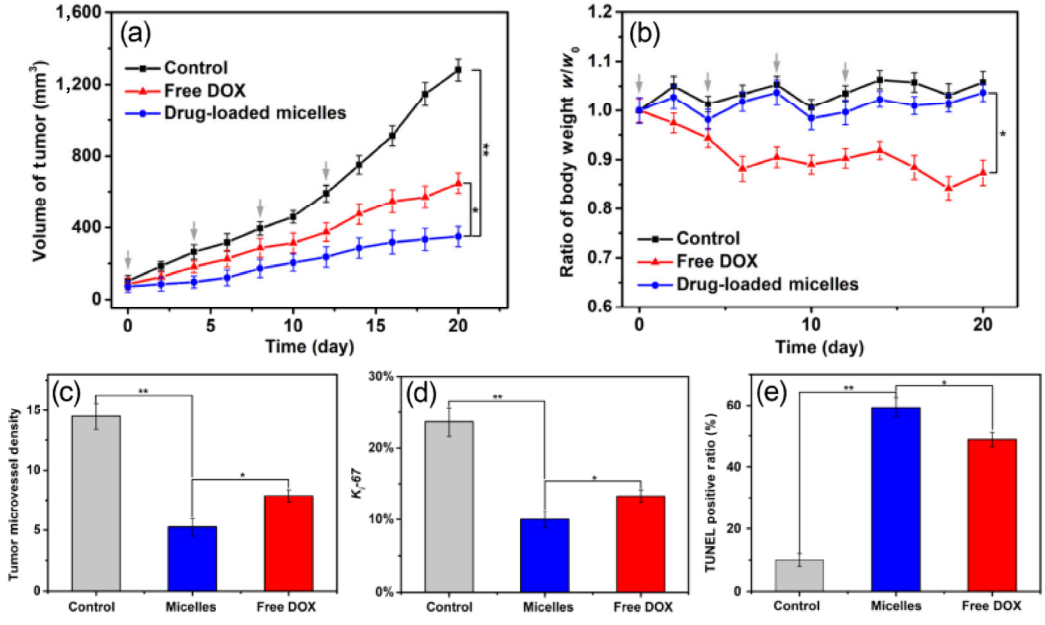

Figure 9 (a) The volumes of tumors treated with PAEE$_{Blink}$-DA micelles, free DOX and saline (control group) over 21 days (*p < 0.05, **p < 0.01). (b) Ratio of body weights (real-time weight / initial weight) of the mice treated with PAEE$_{Blink}$-DA micelles, free DOX, and saline (control group) over 21 days (*p < 0.05). (Gray arrows indicated drug dosing regimen with 5 mg DOX/kg body weight). (c) The CD31-positive area was counted with capillary number (**p < 0.01, *p < 0.05). (d) The K_i-67 density in each image was calculated by K_i-67-positive area/total area (**p < 0.01, *p < 0.05). (e) TUNEL-positive staining and the apoptotic indices were measured as the ratio of apoptotic cells to the total tumor cells in each microscopic field view (**p < 0.01, *p < 0.05).

Acknowledgements

This research was financially supported by the National Natural Science Foundation of China (No. 21502129), the National 111 Project of Introducing Talents of Discipline to Universities (No. B16033), China Postdoctoral Science Foundation Funded Project (Nos. 2017M612956 and 2018T110969), the Key Technology Support Program of Sichuan Province (No. 2016SZ0004), and the State Key Laboratory of Polymer Materials Engineering (No. sklpme2018-3-05). We are grateful for the help of Mr. Chenghui Li (Analytical & Testing Center, Sichuan University) taking laser scanning confocal images.

Electronic Supplementary Material: Supplementary material (the synthesis of the materials, CMC determination, histological studies and immunohistochemical analysis) is available in the online version of this article at https://doi.org/10.1007/ s12274-019-2426-4.

References

[1] Ni, Y.; Wu, J. S. Far-red and near infrared bodipy dyes: Synthesis and applications for fluorescent pH probes and bio-imaging. *Org. Biomol. Chem.* **2014**, *12*, 3774–3791.

[2] Keeble, J.; Goh, C. C.; Wang, Y. L.; Weninger, W.; Ng, L. G. Intravital multiphoton imaging of immune cells. In *Advances in Bio-Imaging: From Physics to Signal Understanding Issues*; Loménie, N.; Racoceanu, D.; Gouaillard, A., Eds.; Springer: Berlin, Heidelberg, 2012; pp 3–16.

[3] Hong, Y. N.; Lam, J. W. Y.; Tang, B. Z. Aggregation-induced emission. *Chem. Soc. Rev.* **2011**, *40*, 5361–5388.

[4] Reisch, A.; Klymchenko, A. S. Fluorescent polymer nanoparticles based on dyes: Seeking brighter tools for bioimaging. *Small* **2016**, *12*, 1968–1992.

[5] Yuan, Y. Y.; Kwok, R. T. K.; Tang, B. Z.; Liu, B. Targeted theranostic platinum(IV) prodrug with a built-in aggregation-induced emission light-up apoptosis sensor for noninvasive early evaluation of its therapeutic responses *in situ*. *J. Am. Chem. Soc.* **2014**, *136*, 2546–2554.

[6] Luo, J. D.; Xie, Z. L.; Lam, J. W. Y.; Cheng, L.; Chen, H. Y.; Qiu, C. F.; Kwok, H. S.; Zhan, X. W.; Liu, Y. Q.; Zhu, D. B. et al. Aggregation-induced emission of 1-methyl-1,2,3,4,5-pentaphenylsilole. *Chem. Commun.* **2001**, 1740–1741.

[7] Jayaram, D. T.; Ramos-Romero, S.; Shankar, B. H.; Garrido, C.; Rubio, N.; Sanchez-Cid, L.; Gómez, S. B.; Blanco, J.; Ramaiah, D. *In vitro* and *in vivo* demonstration of photodynamic activity and cytoplasm imaging through TPE nanoparticles. *ACS Chem. Biol.* **2016**, *11*, 104–112.

[8] Theer, P.; Hasan, M. T.; Denk, W. Two-photon imaging to a depth of 1,000 μm in living brains by use of a Ti:Al_2O_3 regenerative amplifier. *Opt. Lett.* **2003**, *28*, 1022–1024.

[9] Helmchen, F.; Denk, W. Deep tissue two-photon microscopy. *Nat. Methods* **2005**, *2*, 932–940.

[10] Jiang, M. J.; Gu, X. G.; Lam, J. W. Y.; Zhang, Y. L.; Kwok, R. T. K.; Wong, K. S.; Tang, B. Z. Two-photon AIE bio-probe with large stokes shift for specific imaging of lipid droplets. *Chem. Sci.* **2017**, *8*, 5440–5446.

[11] Roberts, W. G.; Palade, G. E. Increased microvascular permeability and endothelial fenestration induced by vascular endothelial growth factor. *J. Cell Sci.* **1995**, *108*, 2369–2379.

[12] Luo, Y. P.; Jiang, F.; Cole, T. B.; Hradil, V. P.; Reuter, D.; Chakravartty, A.; Albert, D. H.; Davidsen, S. K.; Cox, B. F.; McKeegan, E. M. et al. A novel multi-targeted tyrosine kinase inhibitor, linifanib (ABT-869), produces functional and structural changes in tumor vasculature in an orthotopic rat glioma model. *Cancer Chemother. Pharmacol.* **2012**, *69*, 911–921.

[13] Larson, D. R.; Zipfel, W. R.; Williams, R. M.; Clark, S. W.; Bruchez, M. P.; Wise, F. W.; Webb, W. W. Water-soluble quantum dots for multiphoton fluorescence imaging *in vivo*. *Science* **2003**, *300*, 1434–1436.

[14] Wang, D.; Su, H. F.; Kwok, R. T. K.; Hu, X. L.; Zou, H.; Luo, Q. X.; Lee, M. M. S.; Xu, W. H.; Lam, J. W. Y.; Tang, B. Z. Rational design of a water-soluble NIR AIEgen, and its application in ultrafast wash-free cellular imaging and photodynamic cancer cell ablation. *Chem. Sci.* **2018**, *9*, 3685–3693.

[15] Ge, Z. S.; Liu, S. Y. Functional block copolymer assemblies responsive to tumor and intracellular microenvironments for site-specific drug delivery and enhanced imaging performance. *Chem. Soc. Rev.* **2013**, *42*, 7289–7325.

[16] Miyata, K.; Christie, R. J.; Kataoka, K. Polymeric micelles for nano-scale drug delivery. *React. Funct. Polym.* **2011**, *71*, 227–234.

[17] Zhao, J. Y.; Zhong, D.; Zhou, S. B. NIR-I-to-NIR-II fluorescent nanomaterials for biomedical imaging and cancer therapy. *J. Mater. Chem. B* **2018,** *6,* 349–365.

[18] Wang, Y.; Wei, G. Q.; Zhang, X. B.; Huang, X. H.; Zhao J. Y.; Guo, X.; Zhou, S. B. Multistage targeting strategy using magnetic composite nanoparticles for synergism of photothermal therapy and chemotherapy. *Small* **2014,** *14,* 1702994.

[19] Fang, J.; Nakamura, H.; Maeda, H. The EPR effect: Unique features of tumor blood vessels for drug delivery, factors involved, and limitations and augmentation of the effect. *Adv. Drug Deliv. Rev.* **2011**, *63*, 136–151.

[20] Sun, Q. H.; Zhou, Z. X.; Qiu, N. S.; Shen, Y. Q. Rational design of cancer nanomedicine: Nanoproperty integration and synchronization. *Adv. Mater.* **2017**, *29*, 1606628.

[21] Stewart, M. P.; Sharei, A.; Ding, X. Y.; Sahay, G.; Langer, R.; Jensen, K. F. *In vitro* and *ex vivo* strategies for intracellular delivery. *Nature* **2016**, *538*, 183–192.

[22] Sanhai, W. R.; Sakamoto, J. H.; Canady, R.; Ferrari, M. Seven challenges for nanomedicine. *Nat. Nanotechnol.* **2008**, *3*, 242–244.

[23] Shi, J. J.; Kantoff, P. W.; Wooster, R.; Farokhzad, O. C. Cancer nanomedicine: Progress, challenges and opportunities. *Nat. Rev. Cancer* **2016**, *17*, 20–37.

[24] Chen, G. Y.; Roy, I.; Yang, C. H.; Prasad, P. N. Nanochemistry and nanomedicine for nanoparticle-based diagnostics and therapy. *Chem. Rev.* **2016**, *116*, 2826–2885.

[25] Peer, D.; Karp, J. M.; Hong, S.; Farokhzad, O. C.; Margalit, R.; Langer, R. Nanocarriers as an emerging platform for cancer therapy. *Nat. Nanotechnol.* **2007**, *2*, 751–760.

[26] Sugihara, S.; Blanazs, A.; Armes, S. P.; Ryan, A. J.; Lewis, A. L. Aqueous dispersion polymerization: A new paradigm for *in situ* block copolymer self-assembly in concentrated solution. *J. Am. Chem. Soc.* **2011**, *133*, 15707–15713.

[27] Wang, S.; Huang, P.; Chen, X. Y. Hierarchical targeting strategy for enhanced tumor tissue accumulation/retention and cellular internalization. *Adv. Mater.* **2016**, *28*, 7340–7364.

[28] Zhang, Y.; Cai, K. M.; Li, C.; Guo, Q.; Chen, Q. J.; He, X.; Liu, L. S.; Zhang, Y. J.; Lu, Y. F.; Chen, X. L. et al. Macrophage-membrane-coated nanoparticles for tumor-targeted chemotherapy. *Nano Lett.* **2018**, *18*, 1908–1915.

[29] Guo, X.; Wei, X.; Jing, Y. T.; Zhou, S. B. Size changeable nanocarriers with nuclear targeting for effectively overcoming multidrug resistance in cancer therapy. *Adv. Mater.* **2015**, *27*, 6450–6456.

[30] Guo, X.; Shi, C. L.; Yang, G.; Wang, J.; Cai, Z. H.; Zhou, S. B. Dual-responsive polymer micelles for target-cell-specific anticancer drug delivery. *Chem. Mater.* **2014**, *26*, 4405–4418.

[31] Huang, Y.; Tang, Z. H.; Zhang, X. F.; Yu, H. Y.; Sun, H.; Pang, X.; Chen, X. S. pH-triggered charge-reversal polypeptide nanoparticles for cisplatin delivery: Preparation and *in vitro* evaluation. *Biomacromolecules* **2013**, *14*, 2023–2032.

[32] Liu, G. Y.; Li, M.; Zhu, C. S.; Jin, Q.; Zhang, Z. C.; Ji, J. Charge-conversional and pH-sensitive PEGylated polymeric micelles as efficient nanocarriers for drug delivery. *Macromol. Biosci.* **2014**, *14*, 1280–1290.

[33] Xu, P. S.; Van Kirk, E. A.; Zhan, Y. H.; Murdoch, W. J.; Radosz, M.; Shen, Y. Q. Targeted charge-reversal nanoparticles for nuclear drug delivery. *Angew. Chem.* **2007**, *119*, 5087–5090.

[34] Lee, E. S.; Gao, Z. G.; Bae, Y. H. Recent progress in tumor pH targeting nanotechnology. *J. Control. Release.* **2008**, *132*, 164–170.

[35] Lu, Y.; Aimetti, A. A.; Langer, R.; Gu, Z. Bioresponsive materials. *Nat. Rev. Mater.* **2016**, *2*, 16075.

[36] Hu, J. M.; Zhang, G. Y.; Ge, Z. S.; Liu, S. Y. Stimuli-responsive tertiary amine methacrylate-based block copolymers: Synthesis, supramolecular self-assembly and functional applications. *Prog. Polym. Sci.* **2014**, *39*, 1096–1143.

[37] Lee, E. S.; Na, K.; Bae, Y. H. Super pH-sensitive multifunctional polymeric micelle. *Nano Lett.* **2005**, *5*, 325–329.

[38] Mindell, J. A. Lysosomal acidification mechanisms. *Annu. Rev. Physiol.*

2012, *74*, 69–86.

[39] Gu, J. X.; Cheng, W. P.; Liu, J. G.; Lo, S. Y.; Smith, D.; Qu, X. Z.; Yang, Z. Z. pH-triggered reversible "stealth" polycationic micelles. *Biomacromolecules* **2008**, *9*, 255–262.

[40] Yoshio, O.; Reiko, A.; Toyoki, K. Reaction of the azomethine moiety buried in bilayer membranes. *Bull. Chem. Soc. Jpn.* **1983**, *56*, 802–808.

[41] Ma, B. X.; Zhuang, W. H.; Wang, Y. N.; Luo, R. F.; Wang, Y. B. pH-sensitive doxorubicin-conjugated prodrug micelles with charge-conversion for cancer therapy. *Acta Biomater.* **2018,** *70*, 186–196.

[42] Zhou, K. J.; Wang, Y. G.; Huang, X. N.; Luby-Phelps, K.; Sumer, B. D.; Gao, J. M. Tunable, ultrasensitive pH-responsive nanoparticles targeting specific endocytic organelles in living cells. *Angew. Chem., Int. Ed.* **2011**, *50*, 6109–6114.

[43] Zhuang, W. H.; Xu, Y. Y.; Li, G. C.; Hu, J.; Ma, B. X.; Yu, T.; Su, X.; Wang, Y. B. Redox and pH dual-responsive polymeric micelles with aggregation-induced emission feature for cellular imaging and chemotherapy. *ACS Appl. Mater. Interfaces* **2018**, *10*, 18489–18498.

[44] Hu, J.; Zhuang, W. H.; Ma, B. X.; Su, X.; Yu, T.; Li, G. C.; Hu, Y. F.; Wang, Y. B. Redox-responsive biomimetic polymeric micelle for simultaneous anticancer drug delivery and aggregation-induced emission active imaging. *Bioconjugate Chem.* **2018**, *29*, 1897–1910.